Neurocomputing 379 (2020) 141–151

Contents lists available at ScienceDirect

Neurocomputing

journal homepage: www.elsevier.com/locate/neucom

Adaptive neural dynamic surface control of mechanical systems using integral terminal sliding mode

Jafar Keighobadi*, Mehran Hosseini-Pishrobat, Javad Faraji

Faculty of Mechanical Engineering, University of Tabriz, 29 Bahman, Tabriz, Iran

ARTICLE INFO

Article history:
Received 13 August 2019
Revised 3 October 2019
Accepted 11 October 2019
Available online 18 October 2019

Communicated by Prof. Yugang Niu

Keywords:
Dynamic surface control
Mechanical systems
Neural networks
Raised-cosine radial basis functions
Terminal sliding mode

ABSTRACT

This paper studies the robust tracking control problem of fully-actuated mechanical systems using a novel integral dynamics surface control (DSC) method. We replace the conventional DSC error surfaces with new nonlinear integral surfaces to generate a quasi-terminal sliding mode (TSM) in the tracking error trajectories. Then, we follow the recursive, Lyapunov-based design procedure of the DSC to obtain the control law. The resultant quasi-TSM adjusts the error convergence rate according to the distance from the origin. To achieve robustness against structural variations of the mechanical system as well as external disturbances, we use nonlinear damping combined with a radial basis function neural network (RBFNN) approximator. The RBFNN adaptively identifies the upper-bound of the uncertainty/disturbances to prevent conservative, high-gain control inputs. Moreover, we use raised-cosine basis functions, which have compact supports, to improve the computational efficiency of the RBFNN. Through Lyapunov-based stability analysis, we show the boundedness and ultimate boundedness of the closed-loop system as well as the TSM-induced convergence of the tracking errors. Detailed numerical simulations support the efficacy of the proposed control method.

1. Introduction

Motivation. Being rooted in the integrator backstepping [1], dynamic surface control (DSC) is a systematic design method for controlling uncertain nonlinear systems [2,3]. Similar to backstepping, DSC tackles a tracking control problem by introducing a set of coordinates that combine the tracking errors with auxiliary control variables. However, unlike backstepping, DSC uses low-pass-filters to avoid direct differentiation of these variables. A number of papers have shown that augmenting the DSC error surfaces with suitable integral terms improves steady-state tracking and robustness [4–7]. The motivation for the present paper stems from [7] where the robustness of the DSC is enhanced significantly by adding nonlinear proportional-integral (PI)-type terms. The generalization with respect to [7] is twofold: (i) we consider a general n-degrees-of-freedom (DOF) mechanical system conforming to Euler–Lagrange equations rather than a 3-DOF gyroscope; (ii) instead of a quasi-sliding mode term defined by hyperbolic tangent functions, we consider a more general structure based on terminal sliding mode (TSM) theory.

Related literature. Based on the variational principles of mechanics, the Euler–Lagrange equations provide an effective mathematical framework for the analysis of many-body, many-DOF systems [8,9]. In this regard, the control problems of mechanical systems have been extensively studied in the literature, in the context of either Euler–Lagrange systems [9] or robotics [10,11]. Hence, numerous control methods are proposed for the tracking problem of fully-actuated mechanical systems. The majority of the reported controllers rely upon feedback linearization and/or proportional-derivative (PD)-type control inspired by the celebrated Slotine and Li controller [9–12]. Using differential geometric methods, Bullo and Murray [13] studied the problem in a coordinate-free manner. In [3, chapter 6], a convex optimization-based dynamic surface controller was proposed and its disturbance attenuation properties were investigated. By applying the tools of convex analysis, Miranda-Villatoro et al. [14] proposed a class of set-valued controllers for the robust tracking control of Euler–Lagrange systems. For constant desired positions, Cruz-Zavala et al. [15] presented a finite-time controller that modifies the intrinsic energy functions of an Euler–Lagrange system.

Conventional sliding mode (SM) theory is based on the stabilization of a linear switching surface that reduces the order of the system dynamics and induces asymptotic stability of the system trajectories [16]. Sliding mode control (SMC) have been used to achieve strong robustness against a wide variety of uncertainties such as deterministic/stochastic disturbances, unknown nonlinear dynamics, and time-varying additive/multiplicative faults in the

* Corresponding author.
E-mail address: Keighobadi@tabrizu.ac.ir (J. Keighobadi).

https://doi.org/10.1016/j.neucom.2019.10.046
0925-2312/

actuators and/or sensors [16–18]. TSM improves upon the conventional SM by incorporating nonlinear switching surfaces that result in the finite-time stability of the sliding motion [19–21]. Different variations of TSM have been used for robust, finite-time, high-precision control of dynamic systems in various applications [19,22]. In the area of robotics and mechanical systems, the merits of the TSM have attracted the attention of researchers. Nonsingular and continuous forms of TSM have been used for robust and finite-time control of rigid manipulators [23,24]. For fully-actuated mechanical systems, some papers have combined TSM with fractional derivatives/integrals to obtain a better convergence speed [25,26].

Inspired by the biological neurons, artificial neural networks (ANNs) – neural networks (NNs) in short – are powerful tools for data clustering, pattern classification, optimization, and universal function approximation [27]. The latter is of particular interest for control community as there exists a vast literature on the adaptive NN approximation-based control of nonlinear systems, for example, see [28–30]. Particularly, the approximation capabilities of NNs provides an effective framework for adaptive control of uncertain mechanical and robotic systems [28]. Sun et al. [31] used Gaussian radial basis functions (RBFs) to design an adaptive SM controller for robot manipulators; the controller is able to estimate the unmeasured joint velocities. Tran and Kang [32] combined radial basis function neural networks (RBFNNs) approximation with TSM for adaptive finite-time control of robot manipulators. Zhou et al. [33] presented a backstepping-based, adaptive RBFNN control for robot manipulators subject to dead-zone nonlinearity in their control inputs. Liu et al. [34] designed an adaptive NN controller, with the optimal dimension of the hidden NN layer, for robot control in task space.

Contribution. The main contribution of this paper is to present a new tracking controller for mechanical systems by combining the merits of DSC, TSM, and RBFNNs. The novelties and distinctive features of the proposed control method, in comparison with the existing ones, are as follows:

- The recursive design structure of DSC, equipped with integral action, enables us to induce a quasi-TSM at the kinematic level of the tracking control. Moreover, the nonlinear integral TSM surface adjusts the convergence rate of the tracking error according to its distance from the origin.
- Instead of signum functions, we use hyperbolic tangent functions to produce the quasi-TSM. Thereby, the TSM error surface is sufficiently differentiable for DSC design purposes, and the chattering issue in the obtained control law is considerably alleviated.
- We tackle the issue of robustness at two levels. First, at the kinematic level, the proposed TSM grants a certain level of robustness to the position tracking error. Second, at the dynamic level, we employ nonlinear damping [1] in the DSC design. At this level, we also use an RBFNN to adaptively estimate the uncertainty upper-bound and to prevent conservative, high-gain control inputs. We note that, from the function approximation perspective, estimation of the upper-bound of the norm of a vector function demands less computational burden than estimating the function itself.
- In the RBFNN, we use raised-cosine basis functions in lieu of the commonly used Gaussian functions. The raised-cosine functions, unlike Gaussians, enjoy the property of having compact supports, resulting in the computational efficiency [35,36]. Besides, the recent paper [37] has shown that RBFs with compact supports can improve adaptive NNs' learning performance by enhancing the level of excitation of their regressors.

Paper organization. The organization of the remainder of this paper is as follows. Section 2 summarizes notation and required mathematical preliminaries. Section 3 states the control problem. Section 4 presents the main results on the integral DSC design. Section 5 contains further results about the TSM-based convergence of the tracking error. Section 6 elaborates a simulation example of controlling a two-link robot arm. Lastly, Section 7 concludes the paper.

2. Notation and preliminaries

2.1. Notation

Throughout this paper, $\mathbb{R}^+$ denotes the set of nonnegative real numbers. We consider the Euclidean n-space, $\mathbb{R}^n$ equipped with its standard topology. $\|.\|$ stands for the vector 2-norm. $col(.,.,\ldots)$ returns a vector stacked by the given arguments. $tr(.)$ gives the trace of a matrix (.). $\lambda_{\min}(.)$ and $\lambda_{\max}(.)$ return the minimum and the maximum eigenvalues of a real symmetric matrix (.), respectively.

2.2. Mathematical preliminaries

Here, we review some important inequalities that we will use for the convergence analysis of TSM.

Lemma 1. *Let $(v_i)_{i=1}^n$ and $(w_i)_{i=1}^n$ be two sequences of real numbers; we have the following inequalities:*

1. *(Jensen's inequality [20,38]) Let $p > q > 0$, then*

$$\left(\sum_{i=1}^{n}|v_i|^p\right)^{\frac{1}{p}} \le \left(\sum_{i=1}^{n}|v_i|^q\right)^{\frac{1}{q}}; \tag{1}$$

2. *(Hölder's inequality [38]) Let $p > 1$ and $p^{-1}+q^{-1}=1$, then*

$$\sum_{i=1}^{n}|v_i w_i| \le \left(\sum_{i=1}^{n}|v_i|^p\right)^{\frac{1}{p}}\left(\sum_{i=1}^{n}|w_i|^q\right)^{\frac{1}{q}}. \tag{2}$$

Lemma 2. *For any $x \in \mathbb{R}$, $a \ge 0$, and $\varepsilon > 0$, we have the inequality*

$$|x|^{a+1} - x|x|^a \tanh\left(\frac{x}{\varepsilon}\right) \le \delta_a \varepsilon^{a+1}, \tag{3}$$

where $\delta_a = y_0^a(2y_0 - a - 1)$ and y_0 is the unique solution of $y_0(1+\tanh(y_0)) = a+1$.

Proof. We obtain, after some algebraic manipulation, the maximum value $\delta_a\varepsilon^{a+1}$ for the function $|x|^{a+1} - |x|^a x\tanh\left(\frac{x}{\varepsilon}\right)$ by setting its derivative to zero to find the extrema. □

For a vector $x \in \mathbb{R}^n$, $a \ge 0$, and $\varepsilon > 0$, we define

$$Tanh_\varepsilon^a(x) := col\left(|x_i|^a \tanh\left(\frac{x_i}{\varepsilon}\right)\right)_{i=1}^n. \tag{4}$$

Lemma 3. *For any vector $x \in \mathbb{R}^n$, $a \ge 0$, $\varepsilon > 0$, and a diagonal positive definite matrix $L \in \mathbb{R}^{n\times n}$, we have*

$$\delta_a'\lambda_{\min}(L)\|x\|^{a+1} - x^\top L Tanh_\varepsilon^a(x) \le \delta_a\varepsilon^{a+1}tr(L), \tag{5}$$

where $\delta_a' = 1$ for $0 \le a \le 1$ and $\delta_a' = 1/\sqrt{n^{a-1}}$ for $a > 1$.

Proof. Let $L = diag(l_i)_{i=1}^n$; applying Lemma 2 to each component of x and taking the sum over all components, we obtain

$$\sum_{i=1}^{n} l_i|x_i|^{a+1} - x^\top L Tanh_\varepsilon^a(x) \le \delta_a\varepsilon^{a+1}\sum_{i=1}^{n} l_i. \tag{6}$$

Now, we use Lemma 1 to obtain a lower bound of $\sum_{i=1}^n l_i|x_i|^{a+1}$ in terms of $\|x\|$ for different values of a:

1. *Case* $a = 1$: By Rayleigh–Ritz inequality, we have

$$\sum_{i=1}^{n} l_i |x_i|^{a+1} \geq \lambda_{\min}(L)\|x\|^2. \tag{7}$$

2. *Case* $0 \leq a < 1$: In Jensen's inequality (1), let $v_i = l_i^{\frac{1}{q}} x_i$, $p = 2$, and $q = a + 1$:

$$\left(\sum_{i=1}^{n} l_i^{\frac{2}{a+1}} |x_i|^2\right)^{\frac{1}{2}} \leq \left(\sum_{i=1}^{n} l_i |x_i|^{a+1}\right)^{\frac{1}{a+1}}. \tag{8}$$

Since $\sum_{i=1}^{n} l_i^{\frac{2}{a+1}} |x_i|^2 \geq \lambda_{\min}^{\frac{2}{a+1}}(L) \sum_{i=1}^{n} |x_i|^2$, we further have

$$\sum_{i=1}^{n} l_i |x_i|^{a+1} \geq \lambda_{\min}(L)\|x\|^{a+1}. \tag{9}$$

3. *Case* $a > 1$: In Hölder's inequality (2), let $v_i = l_i^{\frac{1}{p}} x_i^2$, $w_i = 1$, $p = (a+1)/2$, and $q = (a+1)/(a-1)$:

$$\sum_{i=1}^{n} l_i^{\frac{2}{a+1}} |x_i|^2 \leq \left(\sum_{i=1}^{n} l_i |x_i|^{a+1}\right)^{\frac{2}{a+1}} n^{\frac{a-1}{a+1}}, \tag{10}$$

which gives

$$\sum_{i=1}^{n} l_i |x_i|^{a+1} \geq \frac{\lambda_{\min}(L)}{\sqrt{n^{a-1}}}\|x\|^{a+1}. \tag{11}$$

Combining (6) with (7), (9), and (11), we obtain the inequality (5). □

Lemma 4. *Consider a nonnegative function* $v(.) \in \mathbb{R}^+$ *that satisfies the differential inequality*

$$\dot{v}(t) \leq -\alpha v^a(t) - \beta v^b(t), \tag{12}$$

with $\alpha, \beta > 0$, $0 < a < 1$, *and* $b \geq 1$. *Then, the following statements hold:*

1. *For all* $t_0 \in \mathbb{R}^+, t \geq t_0$, $v(t)$ *decreases monotonically and satisfies the inequality*

$$v^{1-a}(t) F\left(1, \frac{1-a}{b-a}; \frac{b-2a+1}{b-a}; -\frac{\beta}{\alpha} v^{b-a}(t)\right) \leq v^{1-a}(t_0) F\left(1, \frac{1-a}{b-a}; \frac{b-2a+1}{b-a}; -\frac{\beta}{\alpha} v^{b-a}(t_0)\right) - \alpha(1-a)(t-t_0), \tag{13}$$

where $F(.)$ *is Gauss' hypergeometric function.*

2. *Starting from a nonzero initial value* $v(t_0)$, *we have* $v(t) \leq c < v(t_0)$, *for all* $t \geq t_0 + t_c$ *where the reaching time* t_c *is given by*

$$t_c := \frac{v^{1-a}(t_0)}{\alpha(1-a)} F\left(1, \frac{1-a}{b-a}; \frac{b-2a+1}{b-a}; -\frac{\beta}{\alpha} v^{b-a}(t_0)\right) - \frac{c^{1-a}}{\alpha(1-a)} F\left(1, \frac{1-a}{b-a}; \frac{b-2a+1}{b-a}; -\frac{\beta}{\alpha} c^{b-a}\right). \tag{14}$$

Proof. By integration of the differential inequality (12), we have

$$\int_{v(t_0)}^{v(t)} \frac{dv}{\alpha v^a + \beta v^b} \leq -(t - t_0). \tag{15}$$

The integrand in the left-hand side of (15) is a positive function while the right-hand side is negative. Hence, v is monotonically decreasing with respect to t. Furthermore, the change of variable $w = v^{b-a}$ gives

$$\frac{1}{\alpha(b-a)} \int_{v^{b-a}(t_0)}^{v^{b-a}(t)} \frac{w^{\frac{1-b}{b-a}} dw}{1 + \frac{\beta}{\alpha} w} \leq -(t - t_0). \tag{16}$$

Accordingly, the reaching time to the set $v \leq c$ is

$$t_c = \frac{1}{\alpha(b-a)} \int_{c^{b-a}}^{v^{b-a}(t_0)} \frac{w^{\frac{1-b}{b-a}} dw}{1 + \frac{\beta}{\alpha} w} \tag{17}$$

Evaluating the integrals in (16) and (17) by using the formula 3.194.5 of [39] gives the inequality (13) and the reaching time (14), respectively. □

2.3. Function approximation by neural networks

We consider an RBFNN with the input $x = col(x_j)_{j=1}^{n} \in \mathbb{R}^n$, a hidden layer composed of N neurons, and a single output. The output of the network is given by the nonlinear mapping $\theta^\top \phi(x)$ where $\theta \in \mathbb{R}^N$ is the weight vector and $\phi(.) \in \mathbb{R}^N$ is the vector of basis functions. Using raised-cosine functions [35,40], the basis vector is defined as $\phi(x) := col(\phi_i(x))_{i=1}^{N}$ where

$$\phi_i(x) = \prod_{j=1}^{n} \phi_c\left(\frac{x_j - c_{ij}}{\sigma_{ij}}\right), \quad i = 1 : N, \tag{18a}$$

$$\phi_c(z) = \begin{cases} \cos^2\left(\frac{\pi z}{2}\right), & \text{for } |z| \leq 1, \\ 0, & \text{elsewhere.} \end{cases} \tag{18b}$$

The parameters $c_{ij} \in \mathbb{R}$ and $\sigma_{ij} > 0$ determine the position of the center and the width of the ijth raised-cosine function, respectively. The compact support of the ith basis function is $\prod_{j=1}^{n} [c_{ij} - \sigma_{ij}, c_{ij} + \sigma_{ij}]$.

The RBFNNs with non-polynomial, almost everywhere continuous, locally essentially bounded basis functions are universal approximators for continuous functions over compact sets [36,41]. Hence, the raised-cosine RBFNN (18a) can approximate a continuous function on a compact set arbitrarily accurate. More specifically, let $f : \Omega \to \mathbb{R}$ be a continuous function and $\Omega \subset \mathbb{R}^n$ a compact set. For any $\zeta > 0$, there exists a raised-cosine RBFNN, with sufficiently large dimension N, such that the approximation

$$f(x) = \theta^{*\top} \phi(x) + \zeta^*(x) \tag{19}$$

satisfies the error bound, $\sup_{x \in \Omega} |\zeta^*(x)| < \zeta$ for an ideal weight vector $\theta^* \in \mathbb{R}^N$ where [29]

$$\theta^* \in \left\{\theta_{id} \in \mathbb{R}^N \mid \theta_{id} = \arg \min_{\theta \in \mathbb{R}^N} \left(\sup_{x \in \Omega} \left|f(x) - \theta^\top \phi(x)\right|\right)\right\}. \tag{20}$$

3. System dynamics and formulation of the control problem

Consider an n-DOF mechanical system whose configuration space is parameterized by the generalized coordinates, $q_i \in \mathbb{R}$, $i = 1 : n$. Through Euler–Lagrange equations approach, the dynamics of the mechanical system is governed by the following differential equation [10]:

$$M(q)\ddot{q} + C(q, \dot{q})\dot{q} + D(\dot{q}) + G(q) = u + \Delta(q, \dot{q}, w), \tag{21}$$

where $q := [q_1, \ldots, q_n]^\top \in \mathbb{R}^n$ is the vector of generalized coordinates, $\dot{q} := [\dot{q}_1, \ldots, \dot{q}_n]^\top \in \mathbb{R}^n$ is the vector of generalized velocities, $\ddot{q} := [\ddot{q}_1, \ldots, \ddot{q}_n]^\top \in \mathbb{R}^n$ is the vector of generalized accelerations, $M(q) = M^\top(q) \in \mathbb{R}^{n \times n}$ is the inertia matrix, $C(q, \dot{q}) \in \mathbb{R}^{n \times n}$ is the Coriolis/centripetal matrix, $D(\dot{q}) \in \mathbb{R}^n$ is the vector of dissipative forces, $G(q) \in \mathbb{R}^n$ is the vector of gravitational and/or nonlinear stiffness forces, $u \in \mathbb{R}^n$ is the vector of control forces/torques, $w \in \mathbb{R}^{n_w}$ is the vector of external disturbances, and the unknown function $\Delta(q, \dot{q}, w) \in \mathbb{R}^n$ accounts for the effects of unmodeled dynamics and external disturbances. The mechanical system (21) is subject to internal variations and parametric uncertainty. Hence, we assume that

$$\begin{aligned} M(q) &= M_0(q) + \delta M(q), \\ C(q,\dot{q}) &= C_0(q,\dot{q}) + \delta C(q,\dot{q}), \\ D(\dot{q}) &= D_0(\dot{q}) + \delta D(\dot{q}), \\ G(q) &= G_0(q) + \delta G(q), \end{aligned} \tag{22}$$

where the subscript "0" denotes the nominal part and the symbol "δ" stands for the variation from the nominal part. The mechanical system (21) satisfies the following properties that will be used in the control design [9,10].

Property 1. *The inertia matrix $M(q)$ is positive definite for all $q \in \mathbb{R}^n$.*

Property 2. *The matrix $\dot{M}(q) - 2C(q,\dot{q})$ is skew-symmetric for all $(q,\dot{q}) \in \mathbb{R}^{2n}$.*

We make the following assumption about the uncertainty and disturbances of the mechanical system (21).

Assumption 1. (i) The external disturbances are bounded, that is, $\|w(t)\| \le w_0$ for all $t \in \mathbb{R}^+$ and some positive w_0; (ii) there exist continuous positive functions $\Delta_1^+ : \mathbb{R}^{2n} \to \mathbb{R}^+$ and $\Delta_2^+ : \mathbb{R}^{n_w} \to \mathbb{R}^+$ such that the following inequality holds globally:

$$\|\Delta(q,\dot{q},w)\| \le \Delta_1^+(q,\dot{q}) + \Delta_2^+(w). \tag{23}$$

The control goal is to track a desired trajectory $q_d(t) \in \mathbb{R}^n$ by $q(t)$ in the sense that, in addition to the closed-loop stability, the performance measure $\|q(t) - q_d(t)\|$ converges to zero or, at least, to a small compact set around zero as $t \to \infty$. To this end, the controller should be robust against the internal variations (22) and provide a satisfactory performance in the presence of the external disturbances and unmodeled dynamics, $\Delta(q,\dot{q},w)$.

Assumption 2. The desired trajectory $q_d(.)$ is $\mathcal{C}^2$, $q_d(.)$ and $\dot{q}_d(.)$ are available for control purposes, and $(q_d, \dot{q}_d, \|\ddot{q}_d\|) \in \Omega_d \times [-a_d, a_d]$ where $\Omega_d \subset \mathbb{R}^{2n}$ is a compact set and a_d is a positive constant.

4. Integral dynamic surface control

To obtain a suitable tracking error dynamics, using the DSC formulation, we introduce the following tracking errors:

$$e_1 := q - q_d, \tag{24a}$$

$$e_2 := \dot{q} - v_d, \tag{24b}$$

$$e_3 := v_d - \varphi, \tag{24c}$$

$$T\dot{v}_d + v_d = \varphi, \;\; v_d(0) = \varphi(0). \tag{24d}$$

The vector $e_1 \in \mathbb{R}^n$ is a direct measure of the tracking performance, $\varphi \in \mathbb{R}^n$ is an auxiliary control vector, $v_d \in \mathbb{R}^n$ is the low-pass-filtered version of φ, $e_3 \in \mathbb{R}^n$ is the filtering error, and $T \in \mathbb{R}^{n\times n}$ is a positive definite matrix. The intermediary tracking error $e_2 \in \mathbb{R}^n$ is defined to enable a recursive control design.

To improve the robustness of the DSC, we further define the following integral error surfaces:

$$s_1 = e_1 + \mathcal{I}(e_1,t), \tag{25a}$$

$$s_2 = Hs_1 + e_2, \tag{25b}$$

with $H \in \mathbb{R}^{n\times n}$ being a positive semidefinite coupling matrix and

$$\mathcal{I}(e_1,t) := \int_0^t \exp\left(-\lambda(t-\varsigma)\right)\psi(e_1(\varsigma))\, \mathrm{d}\varsigma, \tag{26}$$

$$\psi(e_1) := \sum_{i=1}^{3} L_i Tanh_\varepsilon^{a_i}(e_1), \tag{27}$$

where $\lambda > 0$, $L_i \in \mathbb{R}^{n\times n}$, $i = 1:3$, are diagonal positive definite matrices, $0 < a_1 < 1$, $a_2 \ge 1$, $a_3 = 0$, and $\varepsilon > 0$.

Remark 1. The function $\psi(.)$ is $\mathcal{C}^1$ over $\mathbb{R}^n$. Hence, after twice differentiation of $\mathcal{I}(e_1,t)$, we will still have continuous functions.

Remark 2. The roles of the different terms of the function $\psi(.)$ in the convergence of the tracking error e_1 are as follows. The first $(0 < a_1 < 1)$ and the second $(a_2 > 1)$ terms produce larger gains when e_1 is near and far from the origin, respectively. In the case $a_2 = 1$, the second term generates a uniform gain distribution. The last term $(a_3 = 0)$ is a robustifying term against bounded perturbations.

Remark 3. The role of the exponential term in (26) is to counteract the memory effect of the integration. Mathematically speaking, $\mathcal{I}(e_1,t)$ satisfies the following bound:

$$\|\mathcal{I}(e_1,t)\| \le \frac{1-\exp(-\lambda t)}{\lambda} \sup_{0\le\varsigma\le t} \|\psi(e_1(\varsigma))\|. \tag{28}$$

Remark 4. The proposed DSC reduces to the conventional DSC by setting H and $\psi(.)$ to zero.

Remark 5. Our proposed integral TSM error surface (25a) differs from the commonly known integral SMs (ISMs) in the following aspect. The ISMs are defined over the whole state space, aiming at retrieving the performance under a nominal control law and eliminating the reaching phase [16–18]. The integral TSM is defined only in the kinematical level of the tracking error to shape a TSM in its dynamics.

The DSC design is carried out by the following steps:

Step 1 (stabilization of s_1). We consider the candidate Lyapunov function

$$V_1 = \frac{1}{2}s_1^\top s_1, \tag{29}$$

whose time derivative, along the trajectories of (21), satisfies

$$\dot{V}_1 = s_1^\top(-Hs_1 + s_2 + e_3 + \varphi - \dot{q}_d - \lambda\mathcal{I}(e_1,t) + \psi(e_1)). \tag{30}$$

According to the nonlinear damping [1], we obtain the auxiliary control input as

$$\varphi(e_1,\dot{q}_d,t) = -K_1 s_1 + \lambda\mathcal{I}(e_1,t) - \psi(e_1) + \dot{q}_d. \tag{31}$$

where $K_1 \in \mathbb{R}^{n\times n}$ is a design positive definite matrix. Hence, we have

$$\dot{V}_1 = -s_1^\top(H+K_1)s_1 + s_1^\top(s_2+e_3). \tag{32}$$

Step 2 (stabilization of s_2). Having Property 1 in mind, we consider the second candidate Lyapunov function as

$$V_2 = V_1 + \frac{1}{2}s_2^\top M(q)s_2. \tag{33}$$

Using Property 2, the time derivative of V_2 is obtained as

$$\dot{V}_2 = -s_1^\top(H+K_1)s_1 + s_1^\top e_3 + s_2^\top(u + f + \delta f). \tag{34}$$

where

$$\begin{aligned} f := {} & (I + C_0(q,\dot{q})H - M_0(q)H(H+K_1))s_1 + M_0(q)Hs_2 \\ & + M_0(q)\left(T^{-1}+H\right)e_3 - D_0(\dot{q}) - G_0(q) - C_0(q,\dot{q})v_d, \end{aligned} \tag{35}$$

$$\begin{aligned} \delta f := {} & (\delta C(q,\dot{q})H - \delta M(q)H(H+K_1))s_1 + \delta M(q)Hs_2 \\ & + \delta M(q)\left(T^{-1}+H\right)e_3 - \delta D(\dot{q}) - \delta G(q) \\ & - \delta C(q,\dot{q})v_d + \Delta(q,\dot{q},w). \end{aligned} \tag{36}$$

Let

$$u = -K_2 s_2 - f + u_r, \tag{37}$$

Table 1
Parameters of two-link robot arm [14].

Parameter	Description	True value	Nominal value
m_1	Mass of the first link	1.5 kg	1.6 kg
m_2	Mass of the second link	1.0 kg	0.8 kg
I_1	Moment of inertia of the first link	0.08 kg m^2	0.085 kg m^2
I_2	Moment of inertia of the second link	0.03 kg m^2	0.025kg m^2
l_1	Length of the first link	0.40 m	0.40 m
l_2	Length of the second link	0.30 m	0.30 m
l_{c_1}	Distance between base and center of gravity of the first link	0.20 m	0.15 m
l_{c_2}	Distance between base and center of gravity of the second link	0.20 m	0.25 m

where $K_2 \in \mathbb{R}^{n\times n}$ is a design positive definite matrix and $u_r \in \mathbb{R}^n$ is a robust control term to be designed. Thereby,

$$\dot{V}_2 = -s_1^\top (H+K_1)s_1 + s_1^\top e_3 - s_2^\top K_2 s_2 + s_2^\top (u_r + \delta f). \tag{38}$$

Step 3 (low-pass-filtering dynamics). The low-pass-filtering error satisfies

$$\dot{e}_3 = -T^{-1}e_3 - \ddot{q}_d + \eta(e_1, e_2, e_3, t), \tag{39}$$

where

$$\begin{aligned}\eta(e_1,e_2,e_3,t) &:= \left(\lambda^2 I + \frac{\partial \psi(e_1)}{\partial e_1}\right)\mathcal{I}(e_1,t) - \left(\lambda I + \frac{\partial \psi(e_1)}{\partial e_1}\right)\psi(e_1) \\ &+ \left(K_1 + \frac{\partial \psi(e_1)}{\partial e_1}\right)(-K_1 e_1 - K_1 \mathcal{I}(e_1,t) + e_2 + e_3).\end{aligned} \tag{40}$$

We consider the candidate Lyapunov function

$$V_3 = V_2 + \frac{e_3^\top e_3}{2}. \tag{41}$$

According to (38) and (39), the time derivative of V_3 satisfies the inequality

$$\begin{aligned}\dot{V}_3 \le & -s_1^\top (H+K_1)s_1 + s_1^\top e_3 - s_2^\top K_2 s_2 + s_2^\top (u_r+\delta f) - e_3^\top T^{-1} e_3 \\ & - e_3^\top \ddot{q}_d + e_3^\top \eta(e_1,e_2,e_3,t).\end{aligned} \tag{42}$$

Step 4 (NN approximation). Now, we use NN approximation to compensate for the uncertain term, δf. In this regard, we assume that $(q, \dot{q}) \in \Omega$ with $\Omega \subset \mathbb{R}^{2n}$ being a compact set. To ensure the feasibility of the tracking control problem [2], we further assume that

Assumption 3. The desired trajectory $q_d(.)$ is feasible in the set Ω, that is, $\Omega_d \subseteq \Omega$.

Proposition 1. *There exists a positive continuous function $\varrho : \mathbb{R}^{4n} \to \mathbb{R}^+$ such that the following inequality holds globally:*

$$\|\delta f\| \le \varrho(q, \dot{q}, q_d, \dot{q}_d). \tag{43}$$

Proof. For any $r \in \mathbb{R}^+$, let $\bar{\psi}(r) := \max_{\|e_1\|\le r} \|\psi(e_1)\|$. According to equations (25a), (25b), (31), and Remark 3, we have the inequalities

$$\|s_1\| \le \|e_1\| + \frac{\bar{\psi}(\|e_1\|)}{\lambda}, \tag{44a}$$

$$\|s_2\| \le \|He_1\| + \|e_2\|, \tag{44b}$$

$$\|\varphi(e_1, \dot{q}_d, t)\| \le \|K_1 s_1\| + 2\bar{\psi}(\|e_1\|) + \|\dot{q}_d\|. \tag{44c}$$

Besides, by Eq. (24d), the low-pass-filtering state, v_d satisfies the following bound for all $t \in \mathbb{R}^+$:

$$\begin{aligned}\|v_d(t)\| \le & \exp\left(\frac{-t}{\lambda_{\max}(T)}\right)\|\varphi(e_1(0), \dot{q}_d(0), 0)\| \\ & + \lambda_{\max}(T)\left(1 - \exp\left(\frac{-t}{\lambda_{\max}(T)}\right)\right)\end{aligned}$$

$$\sup_{0\le\varsigma\le t} \|\varphi(e_1(\varsigma), \dot{q}_d(\varsigma), \varsigma)\|. \tag{45}$$

Taking the inequalities (44a)–(44c) and (45) into consideration, the existence of the function $\varrho(.)$ is deduced from Assumption 1 and the triangle inequalities

$$\|e_1\| \le \|q\| + \|q_d\|, \tag{46a}$$

$$\|e_2\| \le \|\dot{q}\| + \|v_d\|, \tag{46b}$$

$$\|e_3\| \le \|v_d\| + \|\varphi\|. \tag{46c}$$

□

Define

$$\rho(q, \dot{q}, q_d, \dot{q}_d) := \varrho^2(q, \dot{q}, q_d, \dot{q}_d). \tag{47}$$

By Young's inequality and Proposition 1, we have

$$s_2^\top \delta f \le \frac{\|s_2\|^2 \rho(q, \dot{q}, q_d, \dot{q}_d)}{2\epsilon} + \frac{\epsilon}{2}, \tag{48}$$

for any positive ϵ. Over the set $\Omega \times \Omega_d$, for some positive ζ, we consider the RBF NN approximation

$$\rho(q, \dot{q}, q_d, \dot{q}_d) = \theta^{*\top}\phi(\chi) + \zeta^*(\chi), \tag{49}$$

with $\chi = col(q, \dot{q}, q_d, \dot{q}_d)$, $\sup_{\chi\in\Omega\times\Omega_d} |\zeta^*(\chi)| \le \zeta$, and an ideal weight vector $\theta^* \in \mathbb{R}^N$. Let $\theta \in \mathbb{R}^N$ be an estimate of θ^*, define $\tilde{\theta} := \theta^* - \theta$, and consider the candidate Lyapunov function

$$V_4 = V_3 + \frac{1}{2}\tilde{\theta}^\top \Gamma^{-1}\tilde{\theta}. \tag{50}$$

where $\Gamma \in \mathbb{R}^{n\times n}$ is a positive definite matrix. Applying the NN approximation (49) and using the nonlinear damping, we set the robust control input to

$$u_r = -\frac{\left(\theta^\top\phi(\chi) + \kappa\right)}{2\epsilon}s_2, \tag{51}$$

where $\kappa \ge \zeta$ is a design positive. Thereby, we have

$$\begin{aligned}\dot{V}_4 \le & -s_1^\top (H+K_1)s_1 + s_1^\top e_3 - s_2^\top K_2 s_2 + \frac{(\zeta-\kappa)}{2\epsilon}s_2^\top s_2 - e_3^\top T^{-1} e_3 \\ & - e_3^\top \ddot{q}_d + e_3^\top \eta(e_1,e_2,e_3,t) + \frac{\epsilon}{2} + \tilde{\theta}^\top\left(\frac{\phi(\chi)}{2\epsilon}\|s_2\|^2 + \Gamma^{-1}\dot{\tilde{\theta}}\right).\end{aligned} \tag{52}$$

According to the last term in the right hand side of (52), we select the NN update law as

$$\dot{\theta} = \Gamma\left(\frac{\phi(\chi)}{2\epsilon}\|s_2\|^2 - \gamma\theta\right), \tag{53}$$

where γ is a design positive.

Step 5 (stability of the error dynamics). In the next theorem, we state the main results regarding the semiglobal stability of the error dynamics. We note that, according to the proof of Proposition 1, $(q, \dot{q}, q_d, \dot{q}_d) \in \Omega \times \Omega_d$ implies that $(e_1, e_2, e_3) \in \Omega_e$

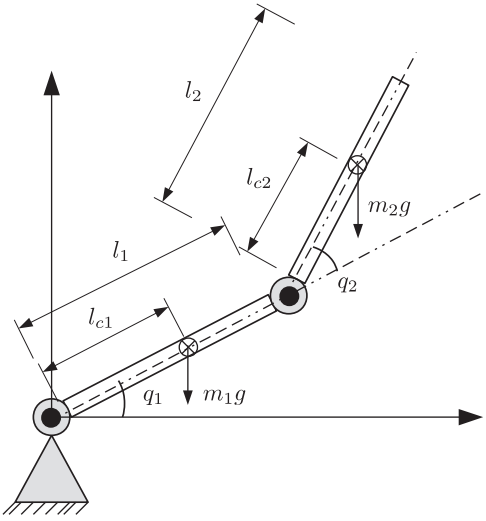

Fig. 1. Schematics of two-link robot arm.

and $(s_1, s_2, e_3) \in \Omega_s$ for some compact sets $\Omega_e \subset \mathbb{R}^{3n}$ and $\Omega_s \subset \mathbb{R}^{3n}$ containing their respective origins.

Theorem 1. *Consider the mechanical system (21) under the adaptive control law given by Eqs. (37), (51), and (53), and assume that Assumptions 1 and 2 hold true. Let $(q, \dot{q}) \in \Omega$ with $\Omega \subset \mathbb{R}^{2n}$ being any compact set satisfying Assumption 3. In the (s_1, s_2, e_3) space, let $\Omega_s \subset \mathbb{R}^{3n}$ be the compact set corresponding to $\Omega \times \Omega_d$. Let $\Omega_\theta \subset \mathbb{R}^N$ be any compact set such that $\{\tilde{\theta} \in \mathbb{R}^N \mid \|\tilde{\theta}\| \le \|\theta^*\|\} \subseteq \Omega_\theta$. Then, all trajectories $(s_1(t), s_2(t), e_3(t), \tilde{\theta}(t))$, $t \in \mathbb{R}^+$, that start in $\Omega_s \times \Omega_\theta$ are bounded and ultimately bounded.*

Table 2
Statistical properties of tracking errors.

Error signal	Conventional DSC		Integral DSC	
	Mean (rad)	RMS (rad)	Mean (rad)	RMS (rad)
$q_1 - q_{1d}$	−0.0302	0.0574	−0.0012	0.0362
$q_2 - q_{2d}$	0.0379	0.0829	0.0017	0.0420

Proof. By Remarks 1 and 3, $\eta(.)$ is upper bounded by a continuous function and there exists a positive η_0 such that $\|\eta(e_1, e_2, e_3, t)\| \le \eta_0$ for all $(e_1, e_2, e_3, t) \in \Omega_e \times \mathbb{R}^+$. As a result, the differential inequality (52) reduces to

$$\dot{V}_4 \le -\bar{\lambda}\left(\|s_1\|^2 + \|s_2\|^2 + \|e_3\|^2\right) - \gamma\|\tilde{\theta}\|^2 + (a_d + \eta_0)\left(\|s_1\|^2 + \|s_2\|^2 + \|e_3\|^2\right)^{\frac{1}{2}} + \gamma\|\theta^*\|\|\tilde{\theta}\| + \frac{\epsilon}{2}, \tag{54}$$

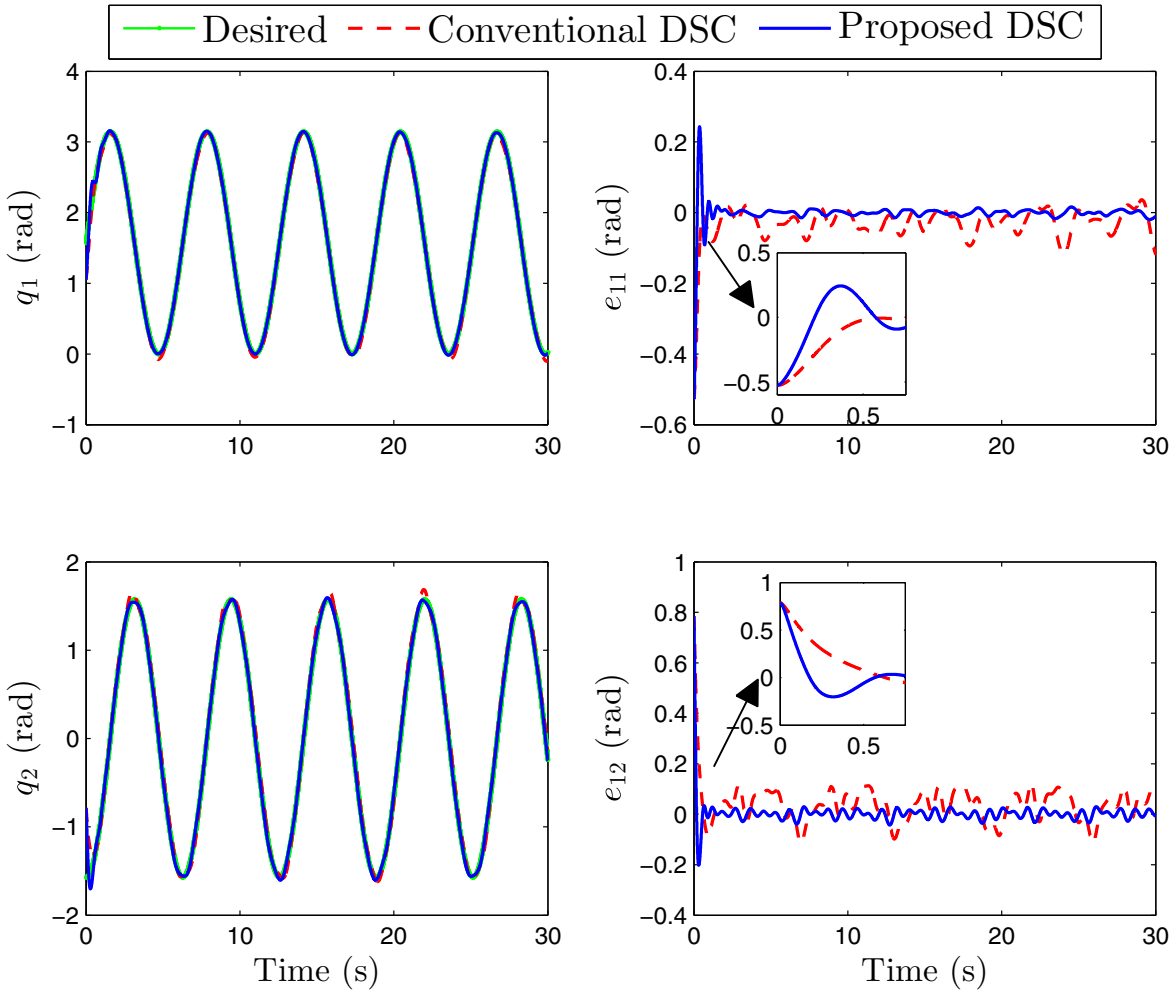

Fig. 2. Tracking performance of the DSC controllers.

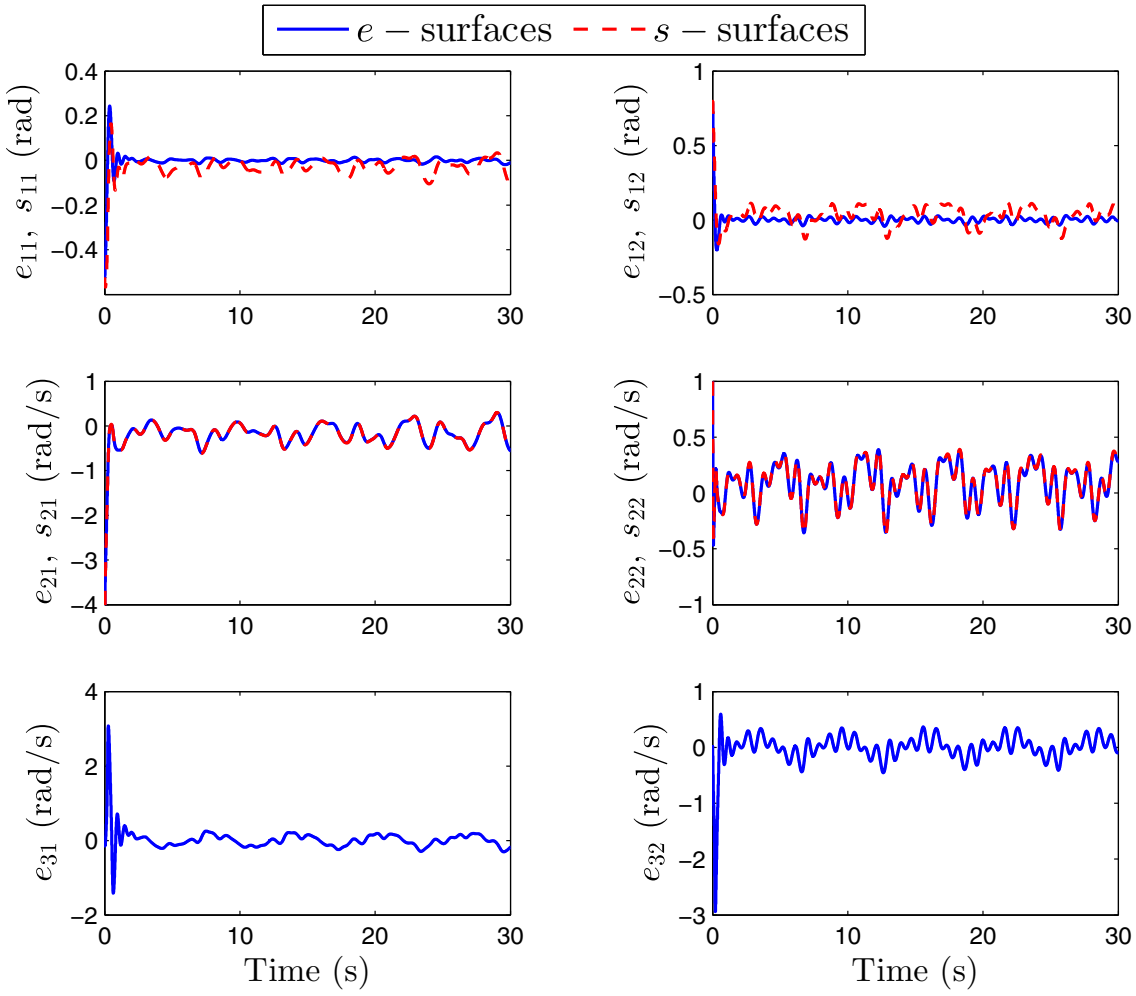

Fig. 3. Time trajectories of the integral DSC error surfaces.

where

$$\bar{\lambda} := \lambda_{\min}\left(\begin{bmatrix} \lambda_{\min}(H+K_1) & 0 & -\frac{1}{2} \\ 0 & \lambda_{\min}(K_2) & 0 \\ -\frac{1}{2} & 0 & \lambda_{\max}^{-1}(T) \end{bmatrix}\right). \tag{55}$$

Assume

$$\lambda_{\min}(H+K_1)\lambda_{\max}^{-1}(T) > \frac{1}{4}, \tag{56}$$

so that $\bar{\lambda} > 0$. Consider the compact set $\bar{\Omega}_s \times \bar{\Omega}_\theta$ where

$$\bar{\Omega}_s := \left\{(s_1, s_2, e_3) \in \mathbb{R}^{3n} \mid \left(\|s_1\|^2 + \|s_2\|^2 + \|e_3\|^2\right)^{\frac{1}{2}} \le r_s\right\}, \tag{57}$$

$$\bar{\Omega}_\theta := \left\{\tilde{\theta} \in \mathbb{R}^N \mid \ \|\tilde{\theta}\| \le \|\theta^*\|\right\}, \tag{58}$$

and

$$r_s := \frac{a_d + \eta_0}{2\bar{\lambda}}\left(1 + \sqrt{1 + \frac{2\epsilon\bar{\lambda}}{(a_d+\eta_0)^2}}\right). \tag{59}$$

We assume the controller parameters are such that, $\bar{\Omega}_s \subseteq \Omega_s$. According to the right-hand side of (54), we have $\dot{V}_4 < 0$ over $\left(\Omega_s \setminus \bar{\Omega}_s\right) \times \left(\Omega_\theta \setminus \bar{\Omega}_\theta\right)$ and $\dot{V}_4 = 0$ on the boundary of $\bar{\Omega}_s \times \bar{\Omega}_\theta$. Thereby, the set $\Omega_s \times \Omega_\theta$ is positively invariant for the $\left(s_1(.), s_2(.), e_3(.), \tilde{\theta}(.)\right)$ trajectories and besides, the trajectories are ultimately bounded with respect to $\bar{\Omega}_s \times \bar{\Omega}_\theta$. The ultimate bound is calculated by finding the smallest level set of the function V_4 that contains $\bar{\Omega}_s \times \bar{\Omega}_\theta$ [42]. That is, after a finite reaching time $t_s \in \mathbb{R}^+$, we have the bounds

$$\|s_1(t)\|^2 + \|s_2(t)\|^2 + \|e_3(t)\|^2 \le \frac{\sqrt{2+\lambda_M^2}r_s^2 + \lambda_{\min}(\Gamma)\|\theta^*\|^2}{\min\{1, \lambda_m\}}, \tag{60}$$

$$\|\tilde{\theta}(t)\|^2 \le \frac{\sqrt{2+\lambda_M^2}r_s^2 + \lambda_{\min}(\Gamma)\|\theta^*\|^2}{\lambda_{\max}(\Gamma)}, \tag{61}$$

where $t \ge t_s$, $\lambda_m := \lambda_{\min}(M(q))$, and $\lambda_M := \lambda_{\max}(M(q))$ over Ω. □

Remark 6. A notable feature of the DSC controller is that it does not require the acceleration of the desired trajectory, $\ddot{q}_d$. This is because of the low-pass-filter (24d) that removes the need for differentiating the auxiliary control input, φ.

5. Tracking error convergence

In Section 4, we designed a dynamic surface controller and established its stability. Now, we further investigate the convergence of the tracking error using the continuous TSM. According to (25a), the dynamics of the tracking error is governed by

$$\dot{e_1} = -\psi(e_1) + \varpi(e_1, e_2, e_3, t), \tag{62}$$

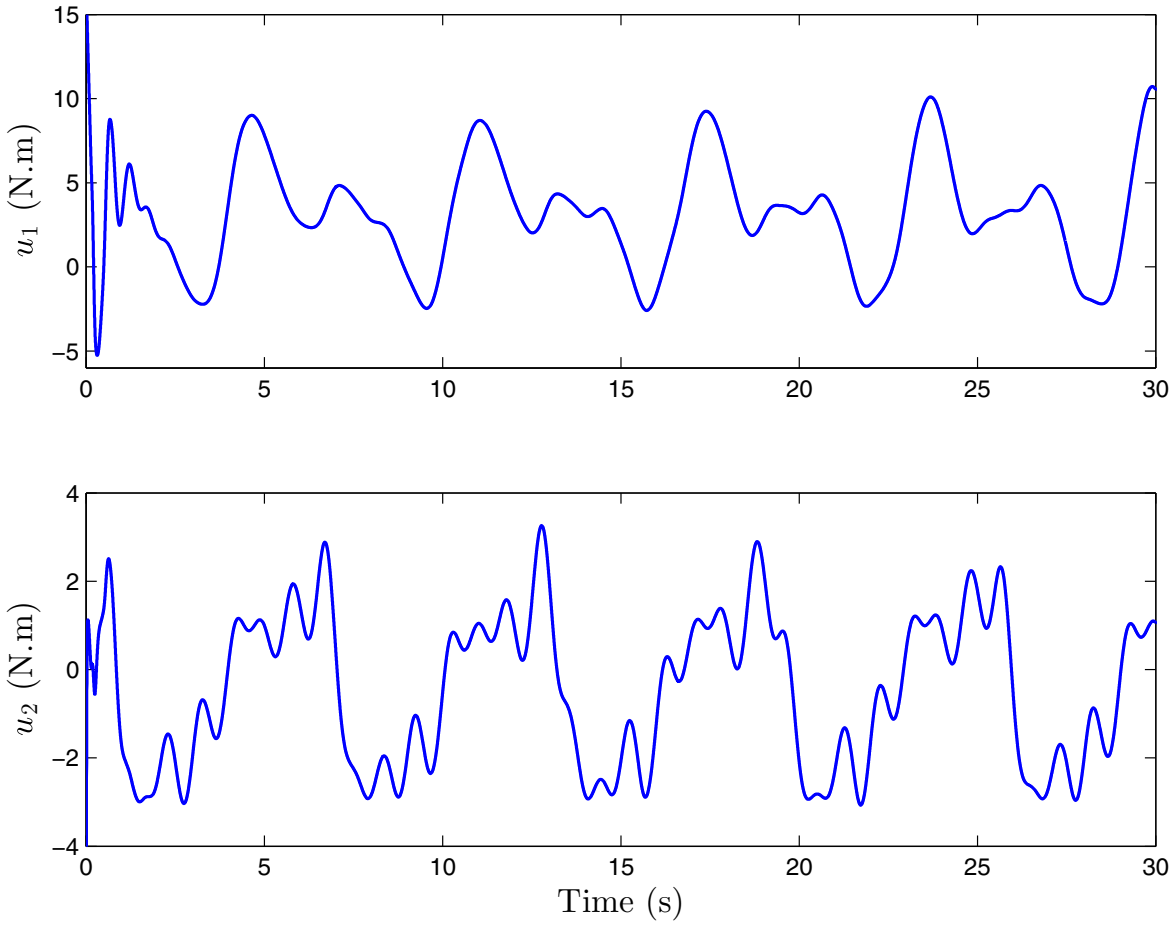

Fig. 4. Control torques generated by the controller.

where

$$\varpi(e_1, e_2, e_3, t) := \lambda \mathcal{I}(e_1, t) - (H + K_1)s_1 + s_2 + e_3. \tag{63}$$

Consider the geometric setting of Theorem 1 and define the compact set

$$\Omega_{e_1} := \Omega_e \cap \left\{(e_1, e_2, e_3) \in \mathbb{R}^{3n} \mid \ e_2 = 0, \ e_3 = 0\right\}, \tag{64}$$

as the projection of Ω_e into the e_1-space.

Theorem 2. *Consider the mathematical setting of Theorem 1 and assume that its conditions and results hold. There exist parameters of the function $\psi(.)$ (27) such that any tracking error trajectory $e_1(.)$, starting in Ω_{e_1}, is ultimately bounded. More specifically, after a transient time $t_r \in \mathbb{R}^+$, the inequality*

$$\|e(t)\| \leq \left(\frac{\sum_{i=1}^{3} \delta_{a_i} \varepsilon^{a_i+1} tr(L_i)}{2(1-\nu)\sqrt{\delta'_{a_1}\delta'_{a_2}\lambda_{\min}(L_1)\lambda_{\min}(L_2)}} \right)^{\frac{2}{a_1+a_2+2}}, \tag{65}$$

holds for $t \geq t_r$ and any number $0 < \nu < 1$; δ_{a_i} and δ'_{a_i} are defined in Lemmas 2 and 3, respectively.

Proof. Since

$$\|\varpi(e_1, e_2, e_3, t)\| \leq \|\psi(e_1)\| + \|(H + K_1)s_1\| + \|s_2\| + \|e_3\|, \tag{66}$$

there exists a positive ϖ_0 such that $\|\varpi(e_1, e_2, e_3, t)\| \leq \varpi_0$ over $\Omega_e \times \mathbb{R}^+$. Considering the positive definite function $V = \frac{e_1^\top e_1}{2}$, differentiating it with respect to time, and using Lemma 3, we get

$$\begin{aligned} \dot{V} \leq & -\delta'_{a_1}\lambda_{\min}(L_1)\|e_1\|^{a_1+1} - \delta'_{a_2}\lambda_{\min}(L_2)\|e_1\|^{a_2+1} \\ & - \left(\delta'_{a_3}\lambda_{\min}(L_3) - \varpi_0\right)\|e_1\| + \mathcal{E}, \end{aligned} \tag{67}$$

where

$$\mathcal{E} := \sum_{i=1}^{3} \delta_{a_i} \varepsilon^{a_i+1} tr(L_i). \tag{68}$$

Assume that

$$\delta'_{a_3}\lambda_{\min}(L_3) \geq \varpi_0, \tag{69}$$

and consider the following set for a $0 < \nu < 1$:

$$\begin{aligned} \Omega_\nu := \Big\{ & e_1 \in \mathbb{R}^n \mid \ \delta'_{a_1}\lambda_{\min}(L_1)\|e_1\|^{a_1+1} \\ & + \delta'_{a_2}\lambda_{\min}(L_2)\|e_1\|^{a_2+1} \leq \frac{\mathcal{E}}{1-\nu} \Big\}. \end{aligned} \tag{70}$$

For $e_1 \in \Omega_{e_1} \setminus \Omega_\nu$, we have the differential inequality

$$\dot{V} \leq -2^{\frac{a_1+1}{2}} \nu \delta'_{a_1}\lambda_{\min}(L_1) V^{\frac{a_1+1}{2}} - 2^{\frac{a_2+1}{2}} \nu \delta'_{a_2}\lambda_{\min}(L_2) V^{\frac{a_2+1}{2}}. \tag{71}$$

According to Lemma 4, $V(e_1(t))$ decreases monotonically outside the set Ω_ν until it enters the minimal level set of V containing Ω_ν. Using the inequality of arithmetic and geometric means, the minimal level set is obtained as

$$\Omega_{e_1}^{\min} := \{e_1 \in \mathbb{R}^n \mid \ V(e_1) \leq c_{\min}\}, \tag{72}$$

where

$$c_{\min} := \frac{1}{2}\left(\frac{\mathcal{E}}{2(1-\nu)\sqrt{\delta'_{a_1}\delta'_{a_2}\lambda_{\min}(L_1)\lambda_{\min}(L_2)}} \right)^{\frac{4}{a_1+a_2+2}}. \tag{73}$$

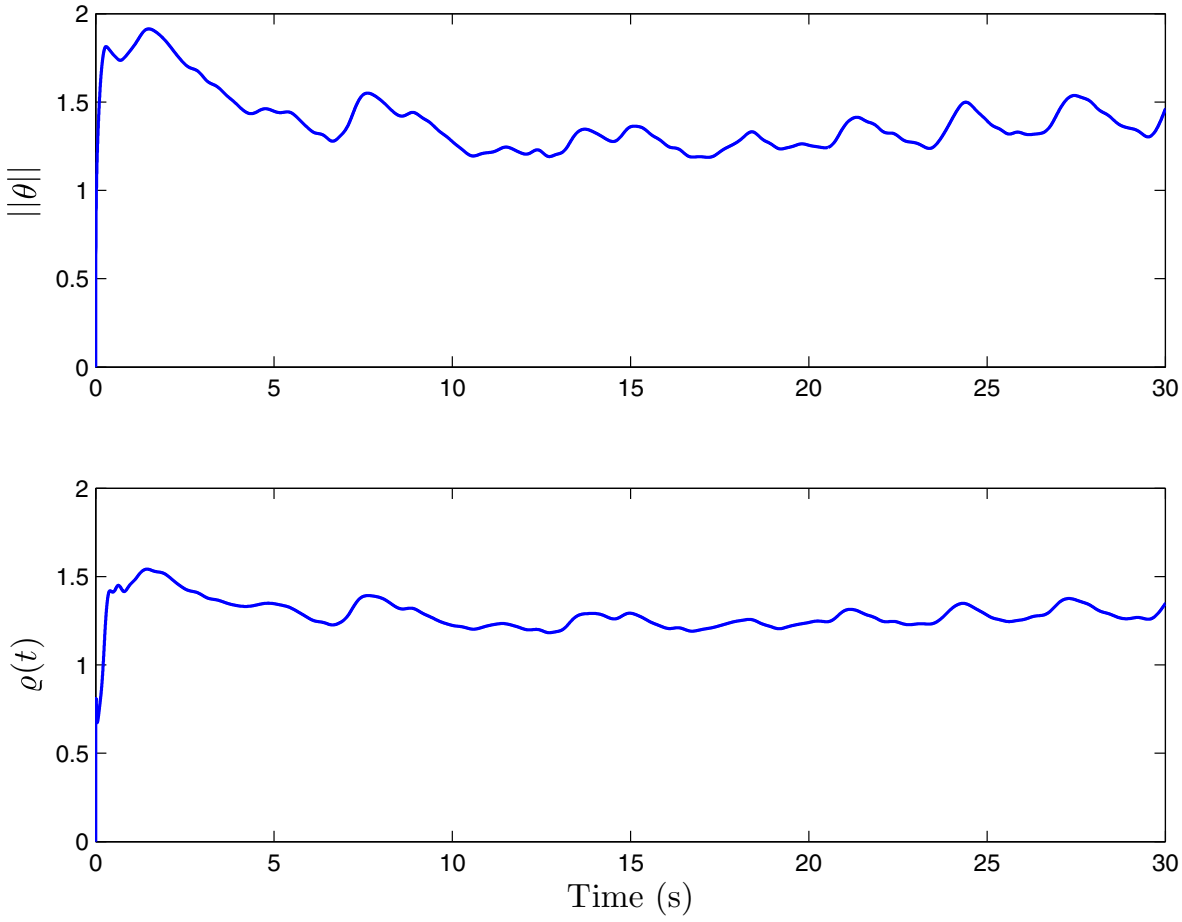

Fig. 5. Neural network weight adaptation (above) and uncertainty bound estimation (below).

Moreover, by Lemma 4, the reaching time to the minimal level set is given by $t_r = t_{c_{\min}}$ where

$$t_{c_{\min}} = \frac{2\sqrt{V^{1-a_1}(0)}}{\sqrt{2^{a_1+1}}\nu\delta'_{a_1}\lambda_{\min}(L_1)(1-a_1)} \times F\left(1, \frac{1-a_1}{a_2-a_1}; \frac{a_2-2a_1+1}{a_2-a_1}; -\frac{\sqrt{2^{a_2-a_1}}\delta'_{a_2}\lambda_{\min}(L_2)}{\delta'_{a_1}\lambda_{\min}(L_1)}\sqrt{V^{a_2-a_1}(0)}\right) - \frac{2\sqrt{c_{\min}^{1-a_1}}}{\sqrt{2^{a_1+1}}\nu\delta'_{a_1}\lambda_{\min}(L_1)(1-a_1)} \times F\left(1, \frac{1-a_1}{a_2-a_1}; \frac{a_2-2a_1+1}{a_2-a_1}; -\frac{\sqrt{2^{a_2-a_1}}\delta'_{a_2}\lambda_{\min}(L_2)}{\delta'_{a_1}\lambda_{\min}(L_1)}\sqrt{V^{a_2-a_1}(0)}\right). \tag{74}$$

Since $\dot{V} \le 0$ on the boundary of $\Omega_{e_1}^{\min}$, the set $\Omega_{e_1}^{\min}$ is positively invariant for the $e_1(.)$ trajectories. This shows that the tracking error trajectories are ultimately bounded and the ultimate bound is $\sqrt{2c_{\min}}$. □

6. Simulation example

6.1. System description

To illustrate the efficacy of the proposed control method, we consider the two-link robot arm depicted in Fig. 1 [14]. The configuration space of the robot is parameterized by the joint angles q_1 and q_2. Through Euler–Lagrange approach, the robot dynamics is obtained as

$$M(q) = \begin{bmatrix} M_{11} & M_{12} \\ M_{12} & M_{22} \end{bmatrix}, \tag{75a}$$

$$\begin{aligned} M_{11} &= m_1 l_{c_1}^2 + m_2\left(l_1^2 + l_{c_2}^2 + 2l_1 l_{c_2}\cos(q_2)\right) + I_1 + I_2, \\ M_{12} &= m_2\left(l_{c_2}^2 + l_1 l_{c_2}\cos(q_2)\right) + I_2, \\ M_{22} &= m_2 l_{c_2}^2 + I_2, \end{aligned}$$

$$C(q,\dot{q}) = -m_2 l_1 l_{c_2}\sin(q_2)\begin{bmatrix} \dot{q}_2 & \dot{q}_1+\dot{q}_2 \\ -\dot{q}_1 & 0 \end{bmatrix}, \tag{75b}$$

$$G(q) = \begin{bmatrix} (m_1 l_{c_1} + m_2 l_1)g\cos(q_1) + m_2 l_{c_2} g\cos(q_1+q_2) \\ m_2 l_{c_2} g\cos(q_1+q_2) \end{bmatrix}, \tag{75c}$$

where $q = [q_1, q_2]^\top$ and $g = 9.81\text{m/s}^2$ is the gravitational acceleration. Table 1 gives the definitions and numerical values of the robot arm parameters. The frictional forces, which are assumed to be unknown in the nominal model, are given by

$$D(\dot{q}) = \frac{1}{2}\begin{bmatrix} \dot{q}_1 + \tanh(\dot{q}_1) \\ \dot{q}_2 + \tanh(\dot{q}_2) \end{bmatrix}. \tag{75d}$$

Furthermore, the uncertain term $\Delta(.)$ is assumed to be

$$\Delta(q,\dot{q},w) = -\begin{bmatrix} \tanh(\dot{q}_1)\sin(q_1+q_2) \\ \tanh(\dot{q}_2)\cos(q_1+q_2) \end{bmatrix} + w, \quad w = \begin{bmatrix} \cos(\pi t)\sin(t) \\ \sin(2\pi t)\cos(t) \end{bmatrix}. \tag{75e}$$

The initial conditions of the robot dynamics are $q(0) = [\pi/3, \pi/3]^\top$ and $\dot{q}(0) = [-\pi/4, \pi/8]^\top$, and the desired trajectory is $q_d(t) = \frac{\pi}{2}[1 + \sin(t), -\cos(t)]^\top$.

6.2. Controller parameters

We consider the nonlinear function (27) with the parameters $a_1 = \frac{1}{2}$, $a_2 = \frac{3}{2}$, $a_3 = 0$, and $\varepsilon = 0.1$. With these parameters, according to the proof of Theorem 2, the hypergeometric function associated with the TSM convergence satisfies

$$F\left(1, \frac{1}{2}; \frac{3}{2}, -z\right) = \frac{\arctan(\sqrt{z})}{\sqrt{z}}, \tag{76}$$

for any $z > 0$ (see Section 9.12 of [39]). We select the gain matrices as $L_1 = diag(1, 1, 1)$, $L_2 = diag(1, 1, 1)$, and $L_3 = diag(1, 1, 1)$. The exponential rate of the integral term (26) is $\lambda = 0.1$. The time constants of the low-pass-filter (24d) are given by $T = diag(0.1, 0.1)$ and the coupling matrix of the integral error surfaces is $H = diag(0.1, 0.1)$. The DSC gain matrices are selected as $K_1 = diag(6, 3)$ and $K_2 = diag(1, 1)$.

To approximate the upper bound function $\varrho(.)$, we consider an RBFNN with $N = 4$ hidden neurons. Taking the ranges of the desired signal and its time derivative into account, we consider the coordinates of the centers as

$$c_{ij} = \begin{cases} \frac{\pi}{2}\left(\frac{i-1}{N-1}\right), & \text{if } j = 1 \text{ or } j = 5, \\ -\frac{\pi}{2} + \frac{\pi}{2}\left(\frac{i-1}{N-1}\right), & \text{otherwise}, \end{cases} \tag{77}$$

for $i = 1 : N$ and $j = 1 : 8$. The width parameter is tuned as $\sigma_{ij} = 3\pi$ for all raised-cosine functions. The gains of the update law (53) are selected as $\Gamma = 1.5I$ and $\gamma = 0.1$, and its initial condition is set to zero. The controller design is completed by considering the robust control term (51) with $\kappa = 1$ and $\epsilon = 0.5$.

6.3. Simulation results

The control system is simulated in the MATLAB/Simulink environment using the fourth-order Runge–Kutta solver with the time step of 1ms. To highlight the effect of the proposed integral TSM design, we also consider the conventional DSC (i.e., $H = O$ and $\psi(.) \equiv 0$). The comparative graph of the tracking performance of the controllers is shown in Fig. 2, and Table 2 gives the mean and root mean square (RMS) values of the tracking errors. We observe that the integral DSC exhibits a better tracking response in terms of mean, energy, and steady-state values of the errors. Besides, the integral DSC has a faster convergence as its transient trajectories have more acute slopes compared to the conventional DSC. But, we note that this results in larger overshoots in the transient phase. The trajectories of the integral DSC surfaces (24a)–(24c) and (25a)–(25b) are depicted in Fig. 3. We see that, in agreement with Theorem 1, the error surfaces are both bounded and ultimately bounded. Besides, as per Theorem 2, the integral TSM improves the convergence of e_1 with respect to s_1. Interestingly, the trajectories of s_1 resemble those of the conventional DSC. The control torques generated by the controller are shown in Fig. 4. Fig. 5 demonstrates the adaptive function approximation performance of the RBFNN in identifying the upper-bound function, $\varrho(.)$.

7. Conclusion

We combined the merits of DSC, TSM, and NN function approximation to present a novel control method for mechanical systems. An integral TSM term is introduced into the conventional DSC design structure. We used RBFNNs with compact supports to adaptively adjust the control gain according to the current magnitude of the disturbances. Comparative simulations showed that the integral DSC outperforms its conventional counterpart in terms of error convergence and robustness. Extending the integral DSC design to more general classes of nonlinear systems is a possible future direction of this research.

Declaration of Competing Interest

The authors declare that they have no known competing financial interests or personal relationships that could have appeared to influence the work reported in this paper.

Acknowledgment

This research was supported by the University of Tabriz's plan to increasing research effectiveness under the contract no. s/858.

References

[1] M. Krstić, I. Kanellakopoulos, P.V. Kokotović, Nonlinear and Adaptive Control Design, Adaptive and Learning Systems for Signal Processing, Communications, and Control, Wiley, New York, 1995.
[2] D. Swaroop, J. Hedrick, P. Yip, J. Gerdes, Dynamic surface control for a class of nonlinear systems, IEEE Trans. Autom. Control 45 (10) (2000) 1893–1899, doi:10.1109/TAC.2000.880994.
[3] B. Song, J.K. Hedrick, Dynamic Surface Control of Uncertain Nonlinear Systems: An LMI Approach, Communications and Control Engineering, Springer, London, 2011, doi:10.1007/978-0-85729-632-0.
[4] L. Zhou, S. Fei, C. Jiang, Adaptive integral dynamic surface control based on fully tuned radial basis function neural network, J. Syst. Eng. Electron. 21 (6) (2010) 1072–1078, doi:10.3969/j.issn.1004-4132.2010.06.021.
[5] W.A. Butt, L. Yan, K. Amezquita S., Adaptive integral dynamic surface control of a hypersonic flight vehicle, Int. J. Syst. Sci. 46 (10) (2015) 1717–1728, doi:10.1080/00207721.2013.828798.
[6] X. Liu, X.-x. Sun, S.-g. Liu, S. Xu, Nonlinear gains recursive sliding mode dynamic surface control with integral action, Asian J. Control 17 (5) (2015) 1955–1961, doi:10.1002/asjc.963.
[7] M. Hosseini-Pishrobat, J. Keighobadi, Extended state observer-based robust non-linear integral dynamic surface control for triaxial MEMS gyroscope, Robotica 37 (3) (2019) 481–501, doi:10.1017/S0263574718001133.
[8] C. Lanczos, The Variational Principles of Mechanics, Dover Books on Physics and Chemistry, fourth ed., Dover Publications, New York, 2012.
[9] R. Ortega, A. Lorá, P.J. Nicklasson, H. Sira-Ramírez, Passivity-Based Control of Euler–Lagrange Systems, Communications and Control Engineering, Springer, London, 1998, doi:10.1007/978-1-4471-3603-3.
[10] R. Kelly, V. Santibáñez, A. Lorá, Control of Robot Manipulators in Joint Space, Advanced Textbooks in Control and Signal Processing, Springer, London, 2005, doi:10.1007/b135572.
[11] M.S. de Queiroz, D.M. Dawson, S.P. Nagarkatti, F. Zhang, Lyapunov-Based Control of Mechanical Systems, Birkhäuser, Boston, MA, 2000, doi:10.1007/978-1-4612-1352-9.
[12] J.-E. Slotine, W. Li, Adaptive manipulator control: a case study, IEEE Trans. Autom. Control 33 (11) (1988) 995–1003, doi:10.1109/9.14411.
[13] F. Bullo, R.M. Murray, Tracking for fully actuated mechanical systems: a geometric framework, Automatica 35 (1) (1999) 17–34, doi:10.1016/S0005-1098(98)00119-8.
[14] F.A. Miranda-Villatoro, B. Brogliato, F. Castanos, Multivalued robust tracking control of Lagrange systems: continuous and discrete-time algorithms, IEEE Trans. Autom. Control 62 (9) (2017) 4436–4450, doi:10.1109/TAC.2017.2662804.
[15] E. Cruz-Zavala, E. Nuno, J.A. Moreno, Continuous finite-time regulation of Euler–Lagrange systems via energy shaping, Int. J. Control (2019) 1–18, doi:10.1080/00207179.2019.1569261.
[16] Y. Shtessel, C. Edwards, L. Fridman, A. Levant, Sliding Mode Control and Observation, Control Engineering, Springer, New York, NY, 2014, doi:10.1007/978-0-8176-4893-0.
[17] A.H. Tahoun, Time-varying multiplicative/additive faults compensation in both actuators and sensors simultaneously for nonlinear systems via robust sliding mode control scheme, J. Frankl. Inst. 356 (1) (2019) 103–128, doi:10.1016/j.jfranklin.2018.08.027.
[18] W. Qi, G. Zong, H.R. Karimi, Sliding mode control for nonlinear stochastic semi-Markov switching systems with application to space robot manipulator model, IEEE Trans. Ind. Electron. (2019) 1, doi:10.1109/TIE.2019.2920619.
[19] X. Yu, M. Zhihong, Fast terminal sliding-mode control design for nonlinear dynamical systems, IEEE Trans. Circuits Syst. I: Fundam. Theory Appl. 49 (2) (2002) 261–264, doi:10.1109/81.983876.
[20] L. Yang, J. Yang, Nonsingular fast terminal sliding-mode control for nonlinear dynamical systems, Int. J. Robust Nonlinear Control 21 (16) (2011) 1865–1879, doi:10.1002/rnc.1666.
[21] Y. Feng, X. Yu, F. Han, On nonsingular terminal sliding-mode control of nonlinear systems, Automatica 49 (6) (2013) 1715–1722, doi:10.1016/j.automatica.2013.01.051.

[22] M. Boukattaya, N. Mezghani, T. Damak, Adaptive nonsingular fast terminal sliding-mode control for the tracking problem of uncertain dynamical systems, ISA Trans. 77 (2018) 1–19, doi:10.1016/j.isatra.2018.04.007.
[23] Y. Feng, X. Yu, Z. Man, Non-singular terminal sliding mode control of rigid manipulators, Automatica 38 (12) (2002) 2159–2167, doi:10.1016/S0005-1098(02)00147-4.
[24] S. Yu, X. Yu, B. Shirinzadeh, Z. Man, Continuous finite-time control for robotic manipulators with terminal sliding mode, Automatica 41 (11) (2005) 1957–1964, doi:10.1016/j.automatica.2005.07.001.
[25] D. Nojavanzadeh, M. Badamchizadeh, Adaptive fractional-order non-singular fast terminal sliding mode control for robot manipulators, IET Control Theory Appl. 10 (13) (2016) 1565–1572, doi:10.1049/iet-cta.2015.1218.
[26] S. Ahmed, H. Wang, Y. Tian, Model-free control using time delay estimation and fractional-order nonsingular fast terminal sliding mode for uncertain lower-limb exoskeleton, J. Vib. Control (2018), doi:10.1177/1077546317750978. 107754631775097
[27] I.N. da Silva, D. Hernane Spatti, R. Andrade Flauzino, L.H.B. Liboni, S.F. dos Reis Alves, Artificial Neural Networks: A Practical Course, Springer International Publishing, Cham, Switzerland, 2017, doi:10.1007/978-3-319-43162-8.
[28] F.L. Lewis, S. Jagannathan, A. Yeşildirek, Neural Network Control of Robot Manipulators and Nonlinear Systems, The Taylor & Francis Systems and Control Book Series, Taylor & Francis, London, 1999.
[29] J.T. Spooner, M. Maggiore, R. Ordóñez, K.M. Passino, Stable Adaptive Control and Estimation for Nonlinear Systems: Neural and Fuzzy Approximator Techniques, John Wiley & Sons, New York, NY, 2004.
[30] J. Farrell, M. Polycarpou, Adaptive Approximation Based Control: Unifying Neural, Fuzzy and Traditional Adaptive Approximation Approaches, Wiley Series in Adaptive and Learning Systems for Signal Processing, Communication and Control, Wiley-Interscience, Hoboken, N.J, 2006.
[31] T. Sun, H. Pei, Y. Pan, H. Zhou, C. Zhang, Neural network-based sliding mode adaptive control for robot manipulators, Neurocomputing 74 (14–15) (2011) 2377–2384, doi:10.1016/j.neucom.2011.03.015.
[32] M.-D. Tran, H.-J. Kang, Adaptive terminal sliding mode control of uncertain robotic manipulators based on local approximation of a dynamic system, Neurocomputing 228 (2017) 231–240, doi:10.1016/j.neucom.2016.09.089.
[33] Q. Zhou, S. Zhao, H. Li, R. Lu, C. Wu, Adaptive neural network tracking control for robotic manipulators with dead zone, IEEE Trans. Neural Netw. Learn. Syst. (2018) 1–10, doi:10.1109/TNNLS.2018.2869375.
[34] C. Liu, Z. Zhao, G. Wen, Adaptive neural network control with optimal number of hidden nodes for trajectory tracking of robot manipulators, Neurocomputing 350 (2019) 136–145, doi:10.1016/j.neucom.2019.03.043.
[35] R. Schilling, J. Carroll, A. Al-Ajlouni, Approximation of nonlinear systems with radial basis function neural networks, IEEE Trans. Neural Netw. 12 (1) (2001) 1–15, doi:10.1109/72.896792.
[36] K.-L. Du, M.N.S. Swamy, Radial basis function networks, in: K.-L. Du, M.N.S. Swamy (Eds.), Neural Networks and Statistical Learning, Springer, London, 2014, pp. 299–335, doi:10.1007/978-1-4471-5571-3_10.
[37] Y. Pan, C. Yang, M. Pratama, H. Yu, Composite learning adaptive backstepping control using neural networks with compact supports, Int. J. Adapt. Control Signal Process. (2019) 1–13, doi:10.1002/acs.3002.
[38] E.F. Beckenbach, R. Bellman, Inequalities, Ergebnisse der Mathematik und ihrer Grenzgebiete, 30, fourth, Springer, Berlin, Heidelberg, 1983, doi:10.1007/978-3-642-64971-4.
[39] I.S. Gradštejn, J.M. Ryžik, V. Moll, Table of Integrals, Series, and Products, eighth, AP, Academic Press/Elsevier, Amsterdam, 2015.
[40] J. Lian, S.H. Żak, Control of uncertain systems, in: S.Y. Nof (Ed.), Springer Handbook of Automation, Springer Handbooks, Springer, Berlin, Heidelberg, 2009, pp. 199–219, doi:10.1007/978-3-540-78831-7_11.
[41] Y. Liao, S.-C. Fang, H.L.W. Nuttle, Relaxed conditions for radial-basis function networks to be universal approximators, Neural Netw. 16 (7) (2003) 1019–1028, doi:10.1016/S0893-6080(02)00227-7.
[42] H.K. Khalil, Nonlinear Control, Pearson, Boston, 2015.

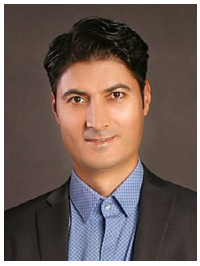

Jafar Keighobadi received the Ph.D. degrees in Mechanical Engineering and Control Systems from Department of Mechanical Engineering, Amirkabir University of Technology, Iran, in 2008. He is currently an Associate Professor of Mechanical Engineering Department at the University of Tabriz. His research interests include artificial intelligence, estimation and identification, nonlinear robust control, and GNC.

Mehran Hosseini-Pishrobat received his B.Sc. and M.Sc. degrees, both in Mechanical Engineering, from the University of Tabriz, Iran, in 2013 and 2016, respectively. Since 2016, he has been a research assistant at the Faculty of Mechanical Engineering, the University of Tabriz. His research interests include nonlinear control, disturbance estimation-based control, and nonlinear observers.

Javad Faraji received his M.Sc. degree in Mechatronic Engineering from the University of Tabriz, Iran. Since 2014, he has been working toward the Ph.D. degree with the Department of Mechanical Engineering, the University of Tabriz. His research interests include integrated navigation systems, estimation and optimization theory, inertial and non-inertial sensors calibration.